Desalination and Water Treatment
www.deswater.com

doi: 10.1080/19443994.2014.979328

57 (2016) 916–932
January

Taylor & Francis
Taylor & Francis Group

Photocatalytic degradation of Tire Cord manufacturing wastewater using an immobilized nanoTiO_2 photocatalytic reactor

M. Habibi[a], A.A.L. Zinatizadeh[a,*], M. Akia[b]

[a]*Faculty of Chemistry, Department of Applied Chemistry, Water and Wastewater Research Center (WWRC), Razi University, Kermanshah, Iran, Tel. +98 9189185612; email: mhabibi1992@gmail.com (M. Habibi), Tel./Fax: +98 8334274559; email: zinatizadeh@gmail.com (A.A.L. Zinatizadeh)*
[b]*Chemistry & Chemical Engineering Research Center of Iran, P.O. Box 14335-186, Tehran, Iran, Tel. +98 218386550; email: akia.mandana@gmail.com*

Received 2 January 2014; Accepted 17 September 2014

ABSTRACT

In this study, an immobilized nanoTiO_2 photocatalyst was developed for the degradation of Tire Cord manufacturing wastewater with low BOD_5/COD ratio (0.1–0.2). The interactive effects of three numerical independent factors (initial COD concentration, initial pH, and reaction time) on the process performance were studied. The process performance was evaluated by monitoring three process responses including COD removal efficiency, specific COD removal rate and BOD_5/COD ratio after treatment. The process was modeled and analyzed using response surface methodology. Maximum COD removal efficiency and BOD_5/COD ratio were modeled to be 38% and 0.5, respectively, at COD_{in} of 350 mg/l and initial pH of 11. The photocatalytic process induced by O_3 and O_3/H_2O_2 showed a remarkable improvement in the process responses studied. Photocatalytic process with sequence regeneration with ozonation could achieve higher COD removal efficiency and BOD_5/COD ratio relative to that obtained from regeneration by aeration.

Keywords: Tire Cord wastewater; Photocatalytic degradation; Immobilized photocatalytic reactor; Titanium dioxide

1. Introduction

Industrial wastewater is one of the important pollution sources in the pollution of the water environment. During the last century, a huge amount of industrial wastewater was discharged into rivers, lakes, and coastal areas. This resulted in serious pollution problems in the water environment and caused negative effects to the eco-system and human's life. The amount of wastewater depends on the technical level of process in each industry sector and will be gradually reduced with the improvement of industrial technologies. The increasing rates of industrial wastewater in developing countries are thought to be much higher than those in developed countries. This fact predicts that industrial wastewater pollution, as a mean environment pollution problem, will move from the developed countries to the developing countries in the early twenty-first century [1]. The complex composition of the industrial wastewater accounts for, in some cases, unpredictable toxicological and ecotoxicological effects [2]. Recalcitrant

---

*Corresponding author.

pollutants are associated with industrial wastewaters which are not typically considered in conventional treatment processes design. Oxidation processes (biological, chemical, or physical) are some of the major steps in wastewater treatment. It is noted that Tire Cord wastewater (TCW) containing non-biodegradable compounds poses a challenge to biological treatment schemes. Biological processes do not normally remove non-biodegradable chemicals, and in some cases, high concentration of such chemicals may inhibit the proper performance of biological processes. Non-biodegradable compounds can be recalcitrant and/or toxic to microorganisms. However, biodegradation is very sensitive to toxic and recalcitrant pollutants and make this method inapplicable [3–6]. For the removal of such disobedient pollutants, traditional physical techniques (adsorption on activated carbon, ultra-filtration, reverse osmosis, incineration, etc.) can generally be used efficiently. Nevertheless, they are non-destructive, since they transfer the contaminant to another phase or location and produce a potentially dangerous and toxic secondary effluent which will leave its own disposal requirement. Consequently, regeneration of the adsorbent materials and post-treatment of solid wastes, which are expensive operations, are needed [7–10]. Chemical methods have been proved to be expensive as they require high dosage of chemicals and produce large quantity of sludge. However, sometimes decomposition by conventional treatments may be difficult. Over the past few years, new technologies have been developed, known as advanced oxidation processes (AOPs). The AOPs are based on the generation of very reactive species—hydroxyl radicals ($OH^\cdot$) that could oxidize wide spectra of organic matter in water and wastewater quickly and non-selectively. Among AOPs, homogeneous and heterogeneous photocatalytic oxidation (PCO) has been demonstrated to be an effective way for removing of non-biodegradable and recalcitrant compounds via a complete mineralization. PCO can be defined as a chemical reaction influenced or initiated by light that removes electrons from a catalyst and adds those electrons to a compound. Semiconducting materials are the key of photocatalytic reaction. The most common semiconductors surveyed for the PCO applications are including: TiO_2, ZnO, CdS, with Fe(III) and precious metals are the most common dopants. TiO_2 has proved to be the most suitable candidate and is the most widely used. The specific features of the TiO_2 consisted of relative inexpensiveness, easy production in large supply, and its high chemical stability which prevent its participating in undesired reactions [11]. In particular, the main advantages of the photocatalytic process are the lack of mass transfer limitations and operating at the ambient conditions [12].

TiO_2 nanoparticles (NPs) are some of the most studied NPs because of their wide range of industrial applications including cosmetics, sunscreens, paints, photovoltaics, and alloys [13]. Because of the practical drawbacks in the use of suspended processes in industrial scales including limited penetration of the radiation in the suspension, fouling of UV source due to the deposition of catalyst particles and separation of the fine solid particles from liquid, immobilization of the catalyst on an inert support would be of vital importance as a practical solution. However the main disadvantage of the immobilized TiO_2 is the over dosage requirement to achieve the same removal efficiency obtained for the TiO_2 powder. Therefore, development of an immobilized photocatalytic reactor (PCR) removing TCW is the novelty of the present research, since the published researches on the AOPs of industrial wastewater mainly focus on the parent compound removal and mineralization, leaving the degradation by-products unexplored. There are some reported studies on the degradation of recalcitrant and toxic compounds by suspended [9,10,12,14,15] and immobilized [16–18] photocatalyst (TiO_2). It is noted that, no study on degradation of TCW in aqueous solution by immobilized PCR has been reported. The present study was designed to determine the degradation of TCW in aqueous solution by UV/TiO_2 photocatalysis and the enhancement of photocatalyst performances by hydrogen peroxide addition and using sequence aeration for reducing the catalyst poisoning.

In this study, relationship between the three numerical independent variables (COD_{in}, reaction time, and initial pH) and three process responses (TCOD removal efficiency, specific COD removal rate (SRR) and final pH) was also determined for the oxidation photocatalytic process of TCW using response surface methodology (RSM).

2. Materials and methods

2.1. Wastewater characteristics

Tire Cord production wastewater was taken from a working Company, Producing Tire Cord, Kermanshah, Iran. The characteristics of the Tire Cord plant wastewater sample are shown in Table 1.

2.2. Experimental setup

A photocatalytic process using immobilized TiO_2 was examined in the treatment of the TCW. In the

Table 1
Characteristics of Tire Cord production wastewater

Parameters	Unit	Amount
TCOD	(mg/l)	450–500
BOD_5	(mg/l)	80–100
TSS	(mg/l)	120–360
pH	–	7–7.8

experiments with photocatalyst, nanotitanium dioxide with anatase structure was coated on the body and inner wall of the quartz tubes with 3 and 5 mm inner and outer diameter, respectively. The configuration of the tubes made was in the form of cylindrical that placed at the surrounding of the UV lamp and was positioned in the center of the vessel (Fig. 1(a) and (b)). Fig. 1(a) represents an image of the applied experimental setup. The number of used tubes was 28 with the height of 20 cm. An air pump ($Q = 0.075\ m^3/min$) was used for the air supply of the cylindrical vessel. The source of UV irradiation was a UV lamp (HITACHI, emission: 365 nm, constant intensity 60 mW/cm^2) that was protected by a quartz jacket and positioned in the center of the reactor. The lighted length of the lamp was 452 mm with a quartz sleeve diameter of 3 cm. NanoTiO_2 loaded in the system was measured 0.314 g catalyst for the 28 quartz tubes (0.3927 g/l).

2.3. Photocatalyst reactor operation

In a typical photocatalytic run, 800 mL of the aqueous solution containing the desired concentration of TCW was loaded in the photocatalyst reactor (PCR). After that, the UV lamp was turned on, while air was continuously sparged in the reaction mixture. Experiments were performed at selected solution pH; the pH of the solution was adjusted to 3, 7, and 11. Adjusting the initial pH (wherever it is required) was done by adding the appropriate amount of 1 M NaOH or 1 M HCl solutions, as necessary.

In order to evaluate the synergistic effects of O_3 and H_2O_2 with the photocalalytic process, the photocatalytic ozonation ($O_3/UV/TiO_2$) and photocatalytic perozonation ($O_3/H_2O_2/UV/TiO_2$) were also examined for the treatment of TCW. The image of photocatalyst ozonation setup is presented in Fig. 1. The air flow rate was set at 5 l/min. The ozone content of the input air stream was measured as 0.27 gO_3/h. The ozone of off-gas was also measured, and the consumed ozone was obtained (2.3 g $ozone_{consumed}/gCOD_{removed}$).

The photocatalytic reaction at the optimum condition was repeated with regular sequence regeneration using aeration and ozonation (every 30 min). This experiment was carried out using raw samples of TCW with COD content of 350 mg/l and pH 3. After every 30 min of the reaction, the photocatalyst was regenerated with aeration or ozonation and distilled water.

2.4. Experimental design

The effects of three independent numerical factors, initial COD concentration, initial pH, and reaction time on the PCR performance were investigated. The experimental range and the levels of the independent variables are shown in Table 2. The central composite face-centered design of the RSM used for designing the parameters. The photocatalytic process was assessed based on the full face-centered CCD experimental design. The design consisted of 2^k factorial points augmented by 2 k axial points and a center point (middle level) where k is the number of variables. The three operating variables were considered at three levels namely, low (−1), middle (0), and high (+1). Accordingly, 20 experiments were conducted with 15 experiments organized in a factorial design (including 8 factorial points, 6 axial points, and 1 center point) and the remaining 5 involving the replication of the middle level to get good estimate of experimental error. Table 3 shows the experimental conditions for the photocatalytic process. COD removal, SRR, BOD_5/COD ratio, and final pH were dependent responses. Data analysis was carried out using general factorial design of the RSM. The results were completely analyzed using analysis of variance (ANOVA) which was performed by Design Expert Software (version 6.0, State-Ease, Inc., Minneapolis, MN).

2.5. Catalyst coating procedure

Quartz tubes washed by water and acetone, then rinsed with deionized (DI) water, and dried. They were finally placed in an electrical furnace at 400℃ for 30 min in order to remove residual organic contaminates and enhance wettability. Wetting is the ability of a liquid to maintain contact with a solid surface, resulting from intermolecular interactions when the two are brought together. The degree of wetting (wettability) is determined by a force balance between adhesive and cohesive forces. Good wettability of a surface is a prerequisite for ensuring good adhesive bonding. A peroxotitanium complex solution was prepared by mixing titanium tetra-iso-propoxide (Merck, purity ≥99.5%), H_2O_2 (Merck, 30%), and H_2O with volume proportions of 12:90:200, respectively. The pH of the solution was then raised to 7.0. The resulting

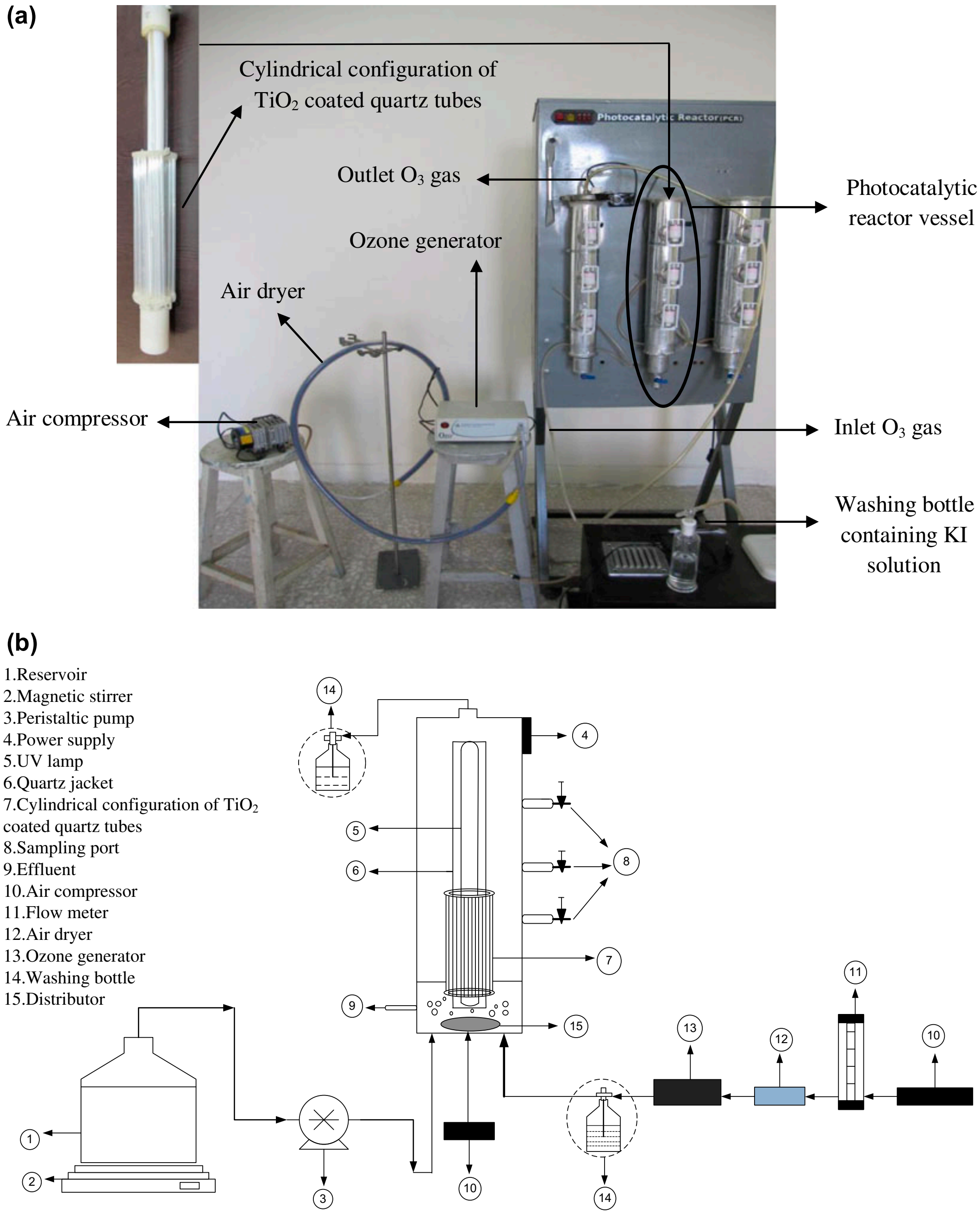

Fig. 1. Laboratory-scale experimental set-up (a) PCR and (b) schematic diagram of the experimental set-up; photocatalytic ozonation system.

solution was refluxed at 90˚C for 10 h to obtain stable anatase phase with controlling the particle sizes. Gel films were formed on the substrates from the 1 wt% TiO_2 sol by dip coating with withdrawal speed of 9.2 mm/s. To control the withdrawal speed, a stepper motor was used for controlling the speed and direction with the change of rpm. For all the samples, a pre-coating of the peroxotitanium complex solution (the sol before reflux) was applied to enhance the adhesion. Subsequent layers of crystalline TiO_2 were deposited by dip coating four times. The samples were dried after each dip at 100˚C for 15 min. Finally, the samples were annealed in the range between 100 and 500˚C for 1 h in air using an electric furnace (Azar Furnaces M2L 1200) [19,20]. The thickness of TiO_2 films was estimated to be 330 ± 5 nm.

Table 2
Experimental range and levels of the independent variables

Variables	Range and levels		
	−1	0	+1
A-Initial COD con.	200	350	500
B-Reaction time	20	130	240
C-Initial pH	3	7	11

2.6. Characterization of TiO_2 coated on quartz tubes

The thin films of TiO_2 coated on the quartz tubes were characterized by scanning electron microscopy (SEM) and atomic force microscope (AFM) to evaluate the surface morphology and the effectiveness of the coating technique. Fig. 2(a) and (b) represents the AFM and SEM images of the nanoTiO_2 coated on the quartz tubes, respectively.

2.6.1. Atomic force microscope

A surface morphology of the coated photocatalyst thin films was visualized using an AFM (Mobile S, Nanosurf, Switzerland). Explorer atomic force microscopy was in the noncontact mode, using high resonant frequency (F0 170 kHz) 15 pyramidal cantilevers with silicon probes having dynamic force. As it can be seen in Fig. 2(a), the AFM image indicated that the film surface is smooth and uniform, and thickness of the film was estimated to be around 330 nm. With an increase in the number of multilayer, the roughness of some parts of the surface increased because of farther deposition of TiO_2 in these sites, which is due to the increase in the amount of TiO_2 deposited per each layer.

2.6.2. Scanning electron microscopy

A surface morphology of titania thin films was studied by scanning electron microscopy using a Philips XL30 microscope at an accelerating voltage of 10 kV. After oven-drying of the thin film for 12 h, the sample was coated with a platinum layer using an SCDOOS sputter coater (BAL-TEC, Sweden) in an argon atmosphere. Subsequently, the sample was scanned and 12 photomicrographs were obtained.

Fig. 2(b) shows the top view of the surface morphology of coated photocatalyst thin films that were examined by scanning electron microscope. A close view surface of the film shows a flat and dense surface morphology of distributed TiO_2 nanoparticles embedded in the film (Fig. 2(b)). The film shows porous structure between the nanoparticles to permit free diffusion of pollutant in and out of the film.

Table 3
Experimental conditions for photocatalytic process

Run No.	Factor 1 *A*: COD in concentration (mg/l)	Factor 2 *B*: Reaction time (min)	Factor 3 *C*: Initial pH
1	200	20	3
2	200	240	3
3	200	130	7
4	200	20	11
5	200	240	11
6	350	130	3
7	350	20	7
8	350	130	7
9	350	130	7
10	350	130	7
11	350	130	7
12	350	130	7
13	350	130	7
14	350	240	7
15	350	130	11
16	500	20	3
17	500	240	3
18	500	130	7
19	500	20	11
20	500	240	11

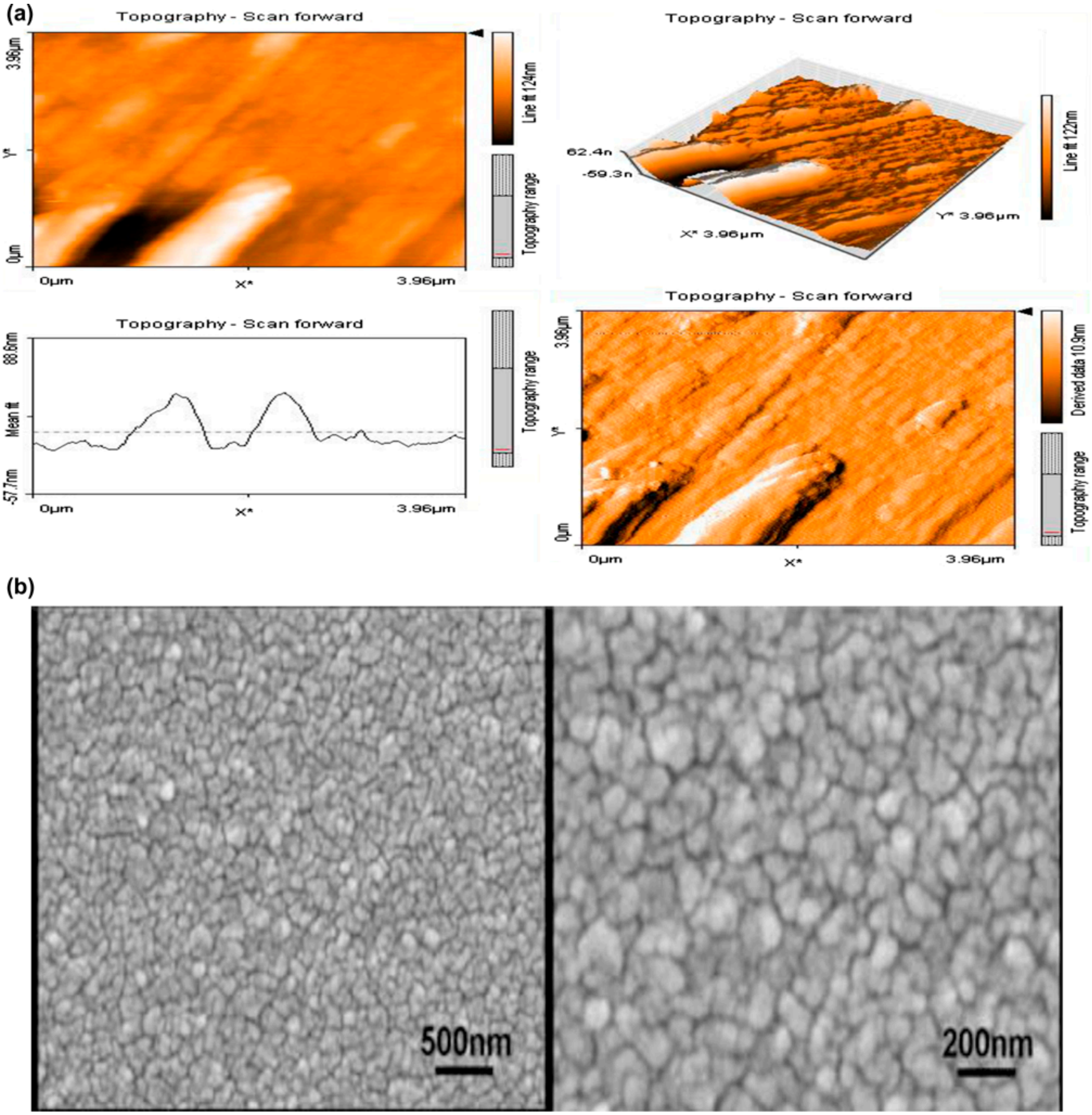

Fig. 2. (a) AFM and (b) SEM images of nano TiO_2 coated, respectively.

2.7. Analytical methods

The samples were analyzed by GC/MS (Agilent 6890 N (0.25 lm, 30 m)) using a capillary column. Oven conditions: 110˚C (2 min) and 200˚C (4 min) with rate of 20˚C/min; 250˚C (2 min) with rate of 40˚C/min. Injector temperature adjusted to 180˚C. Helium (infra, chromatographic purity) was used as carrier gas at pressure of 1 psi. Main products were identified by comparing their mass spectra with those in NIST library. All the chemicals used in the analysis were analytical grade (Merck, Darmstadt, Germany). Chemical oxygen demand (COD) was measured according to the Standard Methods. A colorimetric method with closed reflux method was developed. The closed reflux method is more economical in the use of metallic salt reagents against open reflux. This method is carried out in a 10-ml COD tube. In the colorimetric method, the dichromate ion oxidizes organic material in the sample. This results in the change of chromium from the hexavalent state to the trivalent state. Both these chromium species are colored and absorbed in the visible region of the spectrum. The chromic ion absorbs strongly in the 600-nm region, where the dichromate has nearly zero absorption. Spectrophotometer (DR 5000, Hach, Jenway, USA) at 600 nm was used to measure the absorbance of COD samples. A pH meter (JENWAY 3510) was used for pH measurement. Biodegradability was measured by 5-day biochemical oxygen demand (BOD_5) test in a BOD meter (OxiTop IS 6) according to the Standard Methods [21].

In the runs with H_2O_2, MnO_2 powder was used for elimination of the interference of residual H_2O_2 in COD test. Then, the sample was centrifuged to remove the MnO_2 powders; the supernatant was used for the COD test [16]. The ozone dosage was determined by an iodometric method using a washing bottle containing 2 wt% KI solution [22].

3. Results and discussion

3.1. Process performance

3.1.1. Statistical analysis

ANOVA results for all the responses have been summarized in Table 4. In order to quantify the effects of the factors, the experimental data were fitted to higher degree with the polynomial model. The terms in the equations are presented after the elimination of insignificant variables and their interactions. Based on the statistical analysis, the models were highly significant with very low probability values (<0.0001). It was shown that the model terms of independent variables were significant at the 99% confidence level. The square of correlation coefficient for each response was computed as the coefficient of determination (R^2). It showed high significant regression at ≥93% confidence levels. The value of the adjusted determination coefficient (adjusted R^2) was also high to prove the high significance of the model.

Adequate precision is a measure of the range in predicted response relative to its associated error or, in other words, a signal-to-noise ratio. The noise is defined as the error of the prediction by the models. Its desired value is 4 or more. The value was found more than 20. Simultaneously, low values of the coefficient of variation (CV) (>1%) indicated good precision and reliability of the experiments as suggested by Kuehl [23], and Khuri and Cornell [24]. In order to evaluate repeatability of the performance of the photocatalyst-coated tubes, six repeating runs at middle levels were tested according to the experiments designed by Design Expert software (ver. 7.0). The range of variation in the results showed acceptable repeatability with standard deviation of ±1.29 for COD removal efficiency. The predicted vs. actual plots for the three responses (COD removal, SRR, and final pH) are shown in Fig. 3(a–c), respectively. These plots indicate an adequate agreement between the experimental data and the ones obtained from the models.

3.1.2. COD removal

In this process, COD removal efficiency was calculated as a response representing the process performance in the treatment of the TCW. Relationship between the response and the variables is described by Eq. (1) based on the coded values. According to the Eq. (1), as initial pH (*C*) did not show a significant effect on the response, dependency of the response to the other variables at neutral initial pH was investigated and illustrated by three dimensional plots in Fig. 4.

$$\begin{aligned}\mathrm{COD}_{\mathrm{removal}} = {} & 33.90 - 11.75A + 3.26B - 1.94AC \\ & - 21.19A^2\end{aligned} \tag{1}$$

where *A*, *B*, and *C* are the COD_{in}, the reaction time, and the initial pH, respectively. From the equation, the terms *A* and *B* represented a negative and positive effect on the response, respectively. As it can be seen in Fig. 4, the initial COD concentration showed a reverse impact on the response, an increasing effect at low concentrations (200–350 mg/l) and a decreasing effect at high concentrations (350–500 mg/l). The reaction time showed a slight increasing effect on the response. The same trend was obtained at the other initial pHs (3 and 11). The maximum obtained COD removal efficiency was 38% (corresponding to its actual value 34%) at the COD_{in} of 350 mg/l and the reaction time of 240 min while the minimum response was −3.8% (corresponding to its actual value −6.3%) at the COD_{in} of 500 mg/l and the reaction time of 20 min. The obtained results revealed a significant effect on the response resulted from the initial COD concentration. The low level of COD removal efficiency which obtained at high COD_{in} (500 mg/l) was probably because of an inhibition caused by poisoning of the photocatalyst surface, causing a remarkable reduction in the response. The deactivation of photocatalyst could be attributed to three possible reasons: first, a strong adsorption of the reactant or one of the products on the catalyst surface which leads to the blockage of the some surface sites and consequently decreasing the number of available

Table 4
ANOVA results for response surface models applied

Photocatalytic oxidation									
Response	Modified equations with significant terms	Probability	R^2	AdjR^2	Adeq. precision	SD	CV	Press	Probability for lack of fit
COD removal	$33.90 - 11.75A + 3.26B - 1.94AC - 21.19A^2$	<0.0001	0.9777	0.9716	34.52	2.40	10.29	157.71	0.0994
Final pH	$8.07 + 1.72C + 0.4AC - 0.19B^2 - 0.19C^2$	<0.0001	0.9909	0.9885	61.21	0.14	1.76	0.58	0.2110
SRR	$181.44 - 71.26A - 395.79B + 75.21AB - 201.71A^2 + 225.08B^2 - 96.06C^2 + 328.13A^2B$	<0.0001	0.9298	0.8888	21.88	64.58	44.51	846,986	50,051.79

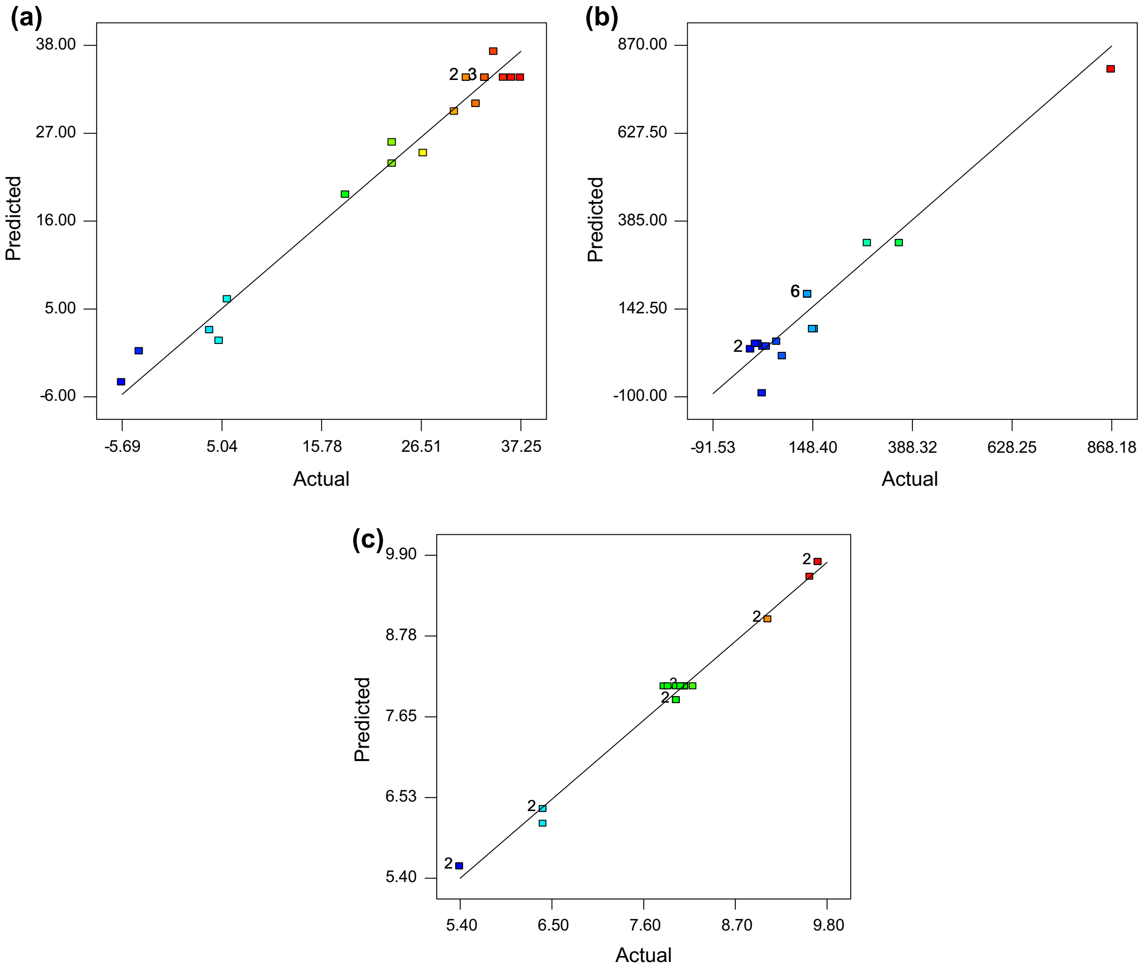

Fig. 3. Predicted vs. actual values plots for (a) COD removal, (b) SRR, and (c) final pH.

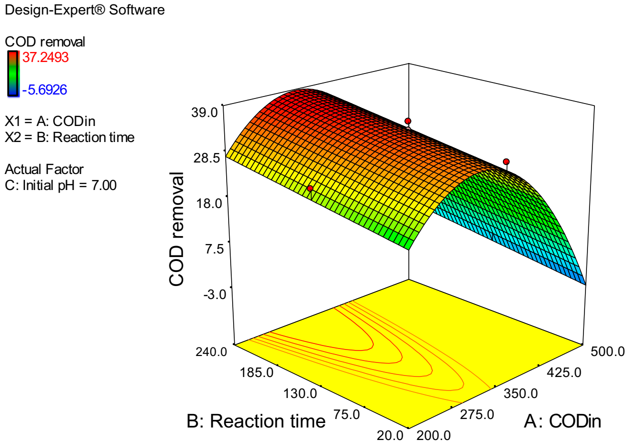

Fig. 4. Response surface plate for COD removal at initial pH 7.

active sites for the adsorption of OH^- anions [17]. Second, the transparency of the solution is decreased with the increase in the initial COD and the UV light absorbed by the organic compounds will be more than that of the photocatalyst [14]. The third possible reason is the interference of the intermediates formed during the degradation of organic compounds in the TCW [25].

A decrease in the response at the low values of COD_{in} also might be attributed to the low concentration of electron donor-organic matter to compensate the electron lost in the photocatalyst hole [26]. This could be because of the low fraction of electron donor-organic content of COD which is resulted from the nature of the TCW. Organic molecules which can adhere effectively to the surface of the photocatalyst will be more susceptible to direct oxidation. Thus, the photocatalytic degradation of aromatics depends on the substituent group. It is reported that nitrophenol is much stronger adsorbing substrate than phenol and therefore is degraded faster. In the degradation of chloroaromatics, it is pointed out that mono-chlorinated phenol is degraded faster than di- or tri-chlorinated members. In general, molecules with electron withdrawing groups such as nitrobenzene and benzoic acid were found to adsorb significantly in the dark compared to those with electron donating groups [27].

The COD removal efficiency at different initial pHs is presented in Fig. 5. As it can be seen in figure, the maximum obtained COD removal efficiencies are 38.2, 34.4, and 37.3%, respectively, in initial pHs of 3, 7, and 11 at 350 mg/l of COD_{in}. In order to clarify the interactive effects of the variables studied, the graphs were prepared as shown in Fig. 6(a–c). Fig. 6(a–c) depicts interactive effects of *AC* (COD_{in}–initial pH) on the COD removal efficiency at different reaction times (*B*). As illustrated in figures, in all the conditions, *C* (initial pH) had a very slight reverse impact in the way that at low COD_{in} it showed a minor increasing effect while it reversed to decreasing at COD_{in} higher than the middle level.

The effect of initial pH on the photocatalytic reactions is related to the surface-charge properties of the photocatalyst and could be explained based on the point of zero charge (pzc). The pzc value for TiO_2 used (Degussa P25) is reported to be at pH 6.25 [27,28]. At pH values lower than pH_{pzc}, the surface became positively charged, and the opposite phenomenon occurred at pH values higher than pH_{pzc}. The highest COD removal efficiency was observed at pH 3 which is attributed to the electrostatic attraction between the positively charged catalyst surface and components anions, leading to the increase of degree of adsorption and photodegradation [29]. The lower degradation rate at higher pH is related to the fact that when the concentration of OH^- is high in the solution; it prevents the penetration of UV light to reach the catalyst surface. Moreover, high value of pH favors the formation of carbonate ions which are effective scavengers of OH^- ions and can reduce the degradation rate [14].

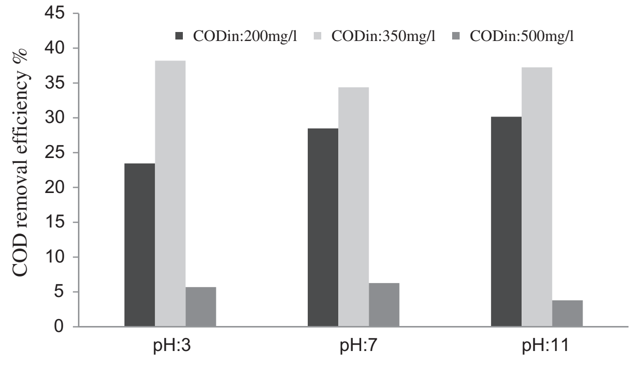

Fig. 5. Performance of different photocatalytic treating TCW.

In order to investigate the trend of COD reduction during the reaction time, the COD-to-COD_0 ratio vs. reaction time was drawn for different COD_{in} concentrations and initial pHs as shown in Fig. 7(a–c). At COD_{in} 500 mg/l, the increase in the ratio at the initial times refers to the presence of some recalcitrant and refractory organic compounds in the TCW (e.g. pyridine 2-ethyl, styrene, pyridine 2-ethenyl, etc.) which are not detected in the COD test [21]. In addition, at the COD_{in} of 350 and 200 mg/l, this ratio continuously decreased which indicates lower concentration of such compounds.

In order to trace the fate of the components, a sample after 240 min from a selected condition (COD_{in} 350 mg/l at pH 11) was analyzed by GC-MS and the results were compared with the raw TCW. Fig. 8(a) and (b) shows the GC-MS chromatogram for the raw and treated samples, respectively. Table 5 presents the peak area obtained from the GC-MS analysis. From the table, the ratio of peak area for a specific compound in treated and raw samples showed degradation percentage achieved. As observed, some of the recalcitrant compounds (e.g. pyridine 2-ethyl and pyridine 2-ethenyl) were disappeared after the photocatalytic process. The other compounds were relatively degraded as shown in Table 5.

SRR was also calculated as another response in this study. A modified cubic model described the variation of the SRR as a function of the variables (COD_{in}, reaction time, and initial pH) in the system (Table 4). Multiple regression coefficients of the model are summarized in Table 4. From the table, *A*, *B*, *AB*, A^2, B^2, C^2, and A^2B are significant model terms in this system. Other model terms are not significant. The following equation describes the relationship between the response and the variables.

$$\begin{aligned}\text{SRR, mgCOD}_{\text{rem}}/\text{gcat h} = {} & 181.44 - 71.26A - 395.79B \\ & + 75.21AB - 201.71A^2 \\ & + 225.08B^2 - 96.06C^2 \\ & + 328.13A^2B \end{aligned} \tag{2}$$

Fig. 9(a) and (b) represents the response surface plots for the SRR as a function of COD_{in} concentration and initial pH at reaction times of 20 and 130 min, respectively. As it can be seen in figures, the COD_{in} concentration had a reverse impact on the response with similar trends as obtained for COD removal. From figures, the initial pH did not show significant effect on the response. As it can be seen in Fig. 9(a) (at reaction time of 20 min), the maximum SRR was found to be 870 mg $\text{COD}_{\text{removed}}$/g cat h at the COD_{in} concentration of

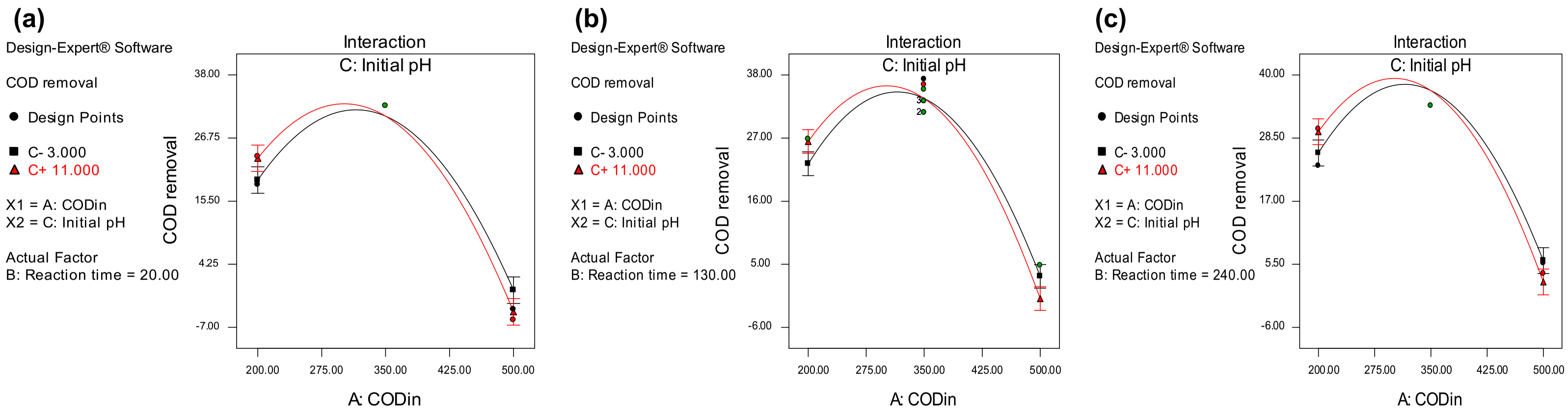

Fig. 6. Interactive effects of AC (COD_{in}–initial pH) on COD removal at different reaction times: (a) 20 min, (b) 130 min, and (c) 240 min.

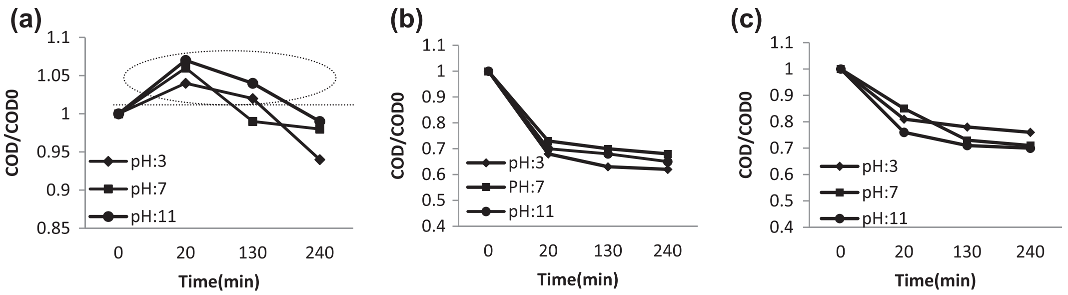

Fig. 7. Changes in COD/COD$_0$ vs. reaction time at different COD$_{in}$ concentration (a) 500, (b) 350, and (c) 200 mg/l.

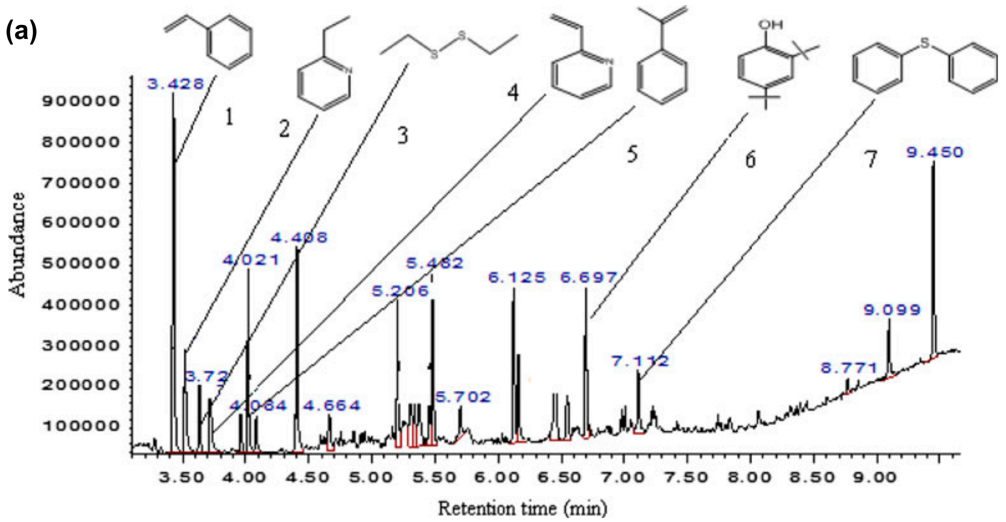

Peak identities are as follows: 1: Styrene, 2: Pyridine 2-ethyl 3: Diethyl disulfide, 4: Pyridine 2- ethenyl, 5: Alpha-methyl styrene, 6: Phenol, 2,4-bis (1,1-dimethylethyl, 7: Diphenyl sulfide

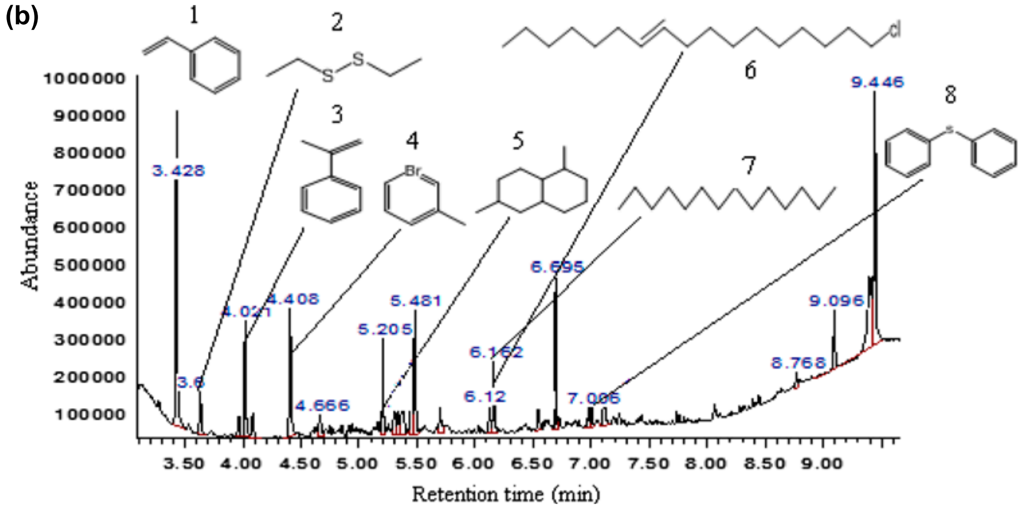

Peak identities are as follows: 1: Styrene, 2: Diethyl disulfide, 3: Alpha methyl styrene, 4: Benzene,1-bromo3-methyl,5: Naphthalene,decahydro-1,6-dimethyl, 6: 7-heptadecene,17 chloro, 7:Tetradecane, 8: Diphenyl sulfide.

Fig. 8. GC-MS analysis of (a) raw TCW and (b) organic contaminants in the oxidized TCW by COD$_{in}$ 350 mg/l at pH 11.

Table 5
Details of GC-MS chromatogram of raw TCW and one treatment process

Type of treatment	Type of component	Peak height	Corr. area	Degradation (%)
Raw sample	Styrene	902,125	9,816,363	–
	Pyridine 2-ethyl	230,586	3,142,783	–
	Pyridine 2-ethenyl	168,635	2,336,464	–
	Diethyl disulfide	145,155	1,484,417	–
	Alpha methyl styrene	425,891	4,157,105	–
	n-Decane	86,184	942,783	–
	Benzene, 1-bromo-3 methyl	511,086	5,637,735	–
	Naphthalene, decahydro-1,6-dimethyl	400,884	4,166,187	–
	Naphthalene, decahydro-2,3-dimethyl	140,133	2,175,645	–
	Cyclo undecene, 1-methyl	204,772	1,837,840	–
	7-Heptadecene, 17-chloro	98,631	1,062,907	–
	Tetradecane	209,160	2,190,089	–
	Phenol, 2,4-bis(1,1-dimethylethyl)	378,149	3,412,067	–
	Diphenyl sulfide	147,090	1,878,328	–
	1-Monolinoleoylglycerol trimethylsilyl ether	36,928	429,615	–
	Heptacosane	487,483	4,861,025	–
COD_{in} 350 mg/l and initial pH 11	Styrene	627,437	7,408,055	24.53
	Diethyl disulfide	109,738	1,167,538	21.35
	Alpha methyl styrene	296,937	3,120,067	24.95
	n-Decane	70,694	806,699	14.43
	Benzene, 1-bromo-3 methyl	325,710	3,718,019	34.05
	Naphthalene, decahydro-1,6-dimethyl	59,001	541,723	86.98
	Naphthalene, decahydro-2,3-dimethyl	112,245	1,772,872	18.51
	Cycloundecene, 1-methyl	163,857	1,477,174	19.62
	7-Heptadecene, 17-chloro	63,148	677,139	36.29
	Tetradecane	172,212	1,567,998	28.40
	Phenol, 2,4-bis(1,1-dimethylethyl)	362,497	3,365,338	1.37
	Diphenyl sulfide	95,448	1,294,184	31.10
	1-Monolinoleoylglycerol trimethylsilyl ether	38,729	350,819	18.34

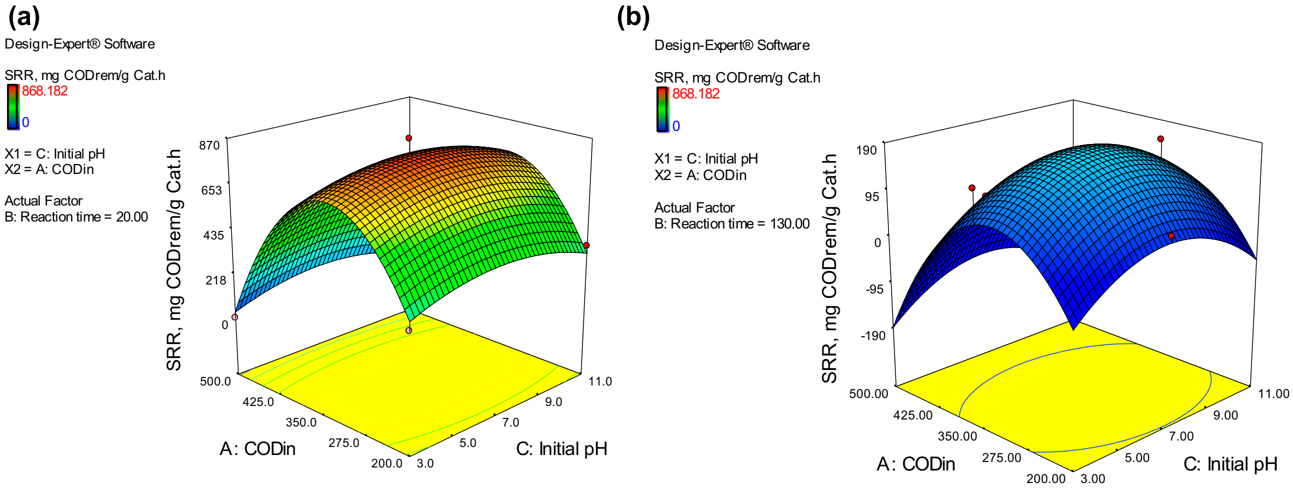

Fig. 9. Response surface plates for specific removal rate at different reaction times (a) 20 and (b) 130 min.

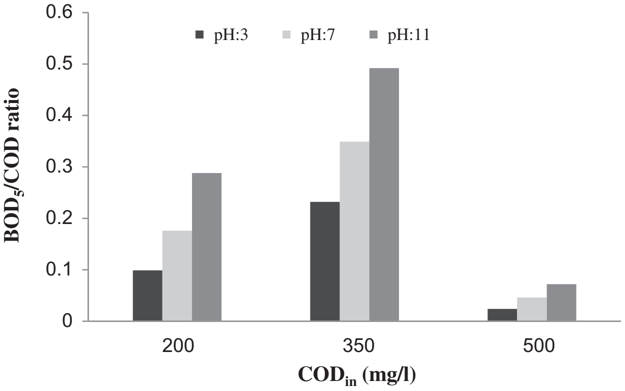

Fig. 10. BOD_5/COD ratio under different conditions studied.

350 mg/l and initial pH of 7 while at reaction time of 130 min (Fig. 9(b)), the maximum SRR was 190 mg $COD_{removed}$/g cat h at the same condition. The remarkable decrease in the SRR value as a result of increasing in the reaction time from 20 to 130 min was probably because of an inhibition resulting from poisoning of the photocatalyst surface.

3.1.3. BOD_5-to-COD ratio

Since one of the aims of applying the PCR is to increase the BOD_5/COD ratio, the ratio was determined at the end of each experiment (after 240 min). The ratio of BOD_5/COD for the raw TCW was determined to be about 0.1–0.2. Fig. 10 presents the BOD_5/COD at different conditions. As it can be seen in figure, the maximum BOD_5-to-COD ratio is about 0.5 at COD_{in} and initial pH of 350 mg/l and 11, respectively. Whereas, the minimum obtained BOD_5/COD is 0.02 for the COD_{in} and initial pH of 500 mg/l and 3, respectively. The trend of ratio changes was compatible with the results obtained for the COD removal efficiency.

Table 6
Order of experiments number according to operating conditions

Run No.	COD_{in} (mg/l)	Initial pH
1	200	3
2		7
3		11
4	350	3
5		7
6		11
7	500	3
8		7
9		11

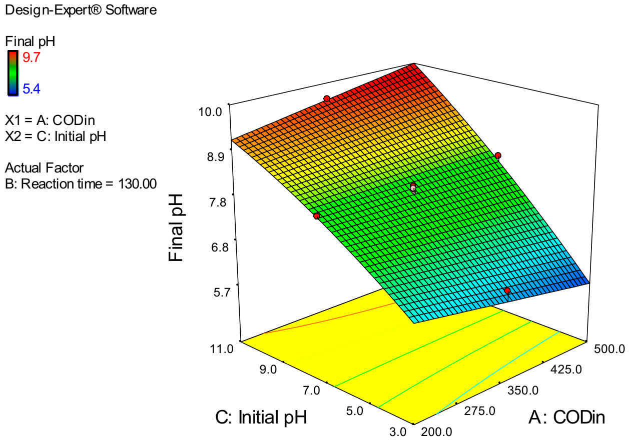

Fig. 12. Response surface plate for final pH at reaction time 240 min.

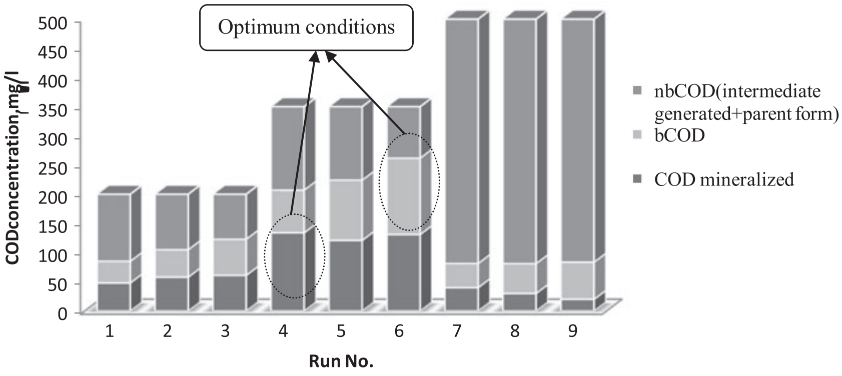

Fig. 11. COD fractionation for the samples after the treatment process.

In order to monitor the fate of the COD contents in the samples after the treatment processes, different fractions of the COD (including COD mineralized, biodegradable COD (bCOD), and non-biodegradable COD (nbCOD)) are represented in Fig. 11. Fig. 11 has been drawn according to the experiments' numbers as presented in Table 6. In this process, the maximum COD removal and BOD-to-COD ratio is explored. As specified in figure, the maximum mineralization and bCOD fraction were observed at the experiments Nos. 4 and 6, respectively (the operating conditions are presented in Table 6). As a result, the maximum bCOD fraction was obtained at initial pH of 11 while the maximum COD mineralization was achieved at acidic initial pH (3).

3.1.4. Final pH

A reduced quadratic model described the variation of the final pH as a function of the variables (COD_{in}, initial pH, and reaction time) (Table 4). Regression coefficients of the model are summarized in Table 4. The following regression equation (built with coded values) was obtained for the variation of the final pH.

$$\text{Final pH} = 8.07 + 1.72C + 0.4AC - 0.19B^2 - 0.19C^2 \quad (3)$$

As seen in Table 4, C, AC, B^2, and C^2 were significant model terms and other model terms are not significant (with a probability value larger than 0.05). Fig. 12 represents the changes in the final pH as a function of COD_{in} and initial pH at the reaction time of 240 min. As illustrated by the model, the most influential factor affecting the final pH is C (initial pH) and the least effect is related to A (COD_{in}). From figure, the COD_{in} has no impact on the process response and initial pH has a mild reverse effect on the response which showed an increasing effect at the range of 3–7 and a decreasing effect at the range of 7–11. The results showed a decrease in the final pH relative to the initial pH which might be attributed to the formation of dicarboxylic acids and the small molecules of organic acids, as well as CO_2 and carbonic acids from complete mineralization of the organic matter [30,31]. The other reason for the decrease in the pH value refers to the mechanisms of the photocatalytic process so that the photogenerated valence band holes react with either water (H_2O) or hydroxyl ions (OH^-) adsorbed on the catalyst surface to generate hydroxyl radicals ($OH^\bullet$) which are strong oxidants according to the following equations [32].

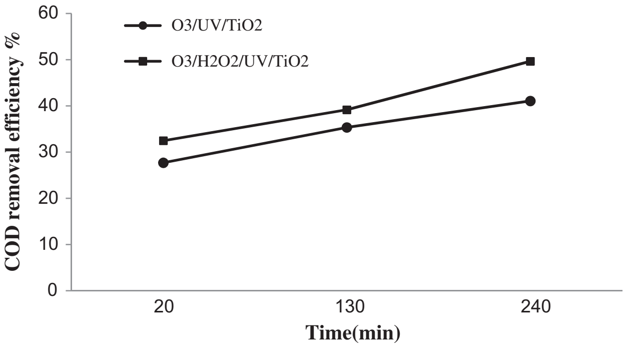

Fig. 13. Performance of the photocatalytic process induced by O_3 and O_3/H_2O_2.

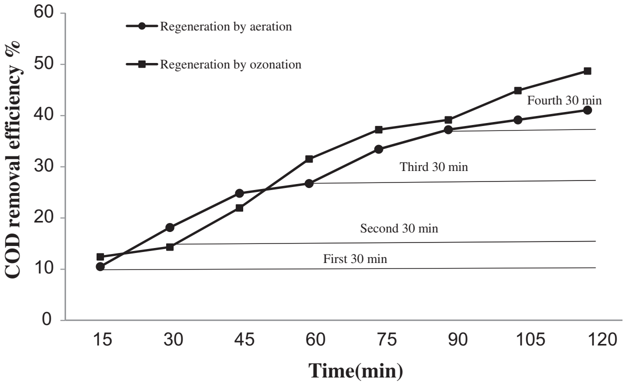

Fig. 14. Performance of photocatalytic process with regular sequence regeneration by aeration and ozonation.

$$TiO_2(h^+) + H_2O \rightarrow TiO_2 + HO^\bullet + H^+ \quad (4)$$

$$TiO_2(h^+) + HO^- \rightarrow TiO_2 + HO^\bullet \quad (5)$$

Conversely, the increase in the pH value is related to the formed electrons that can reduce the dissolved oxygen, creating a superoxide radical ion ($O_2^{\bullet-}$) (reaction 6), which subsequently is converted into H_2O_2 according to the reactions 7 and 8. The hydrogen peroxide also acts as an electron receptor, generating extra hydroxyl radicals and hydroxyl ions (reaction 9).

$$TiO_2(e^-) + O_2 \rightarrow TiO_2 + O_2^{\bullet-} \quad (6)$$

$$O_2^{\bullet-} + H_2O \rightarrow HO_2^\bullet + HO^- \quad (7)$$

$$2\,HO_2^\bullet \rightarrow H_2O_2 + O_2 \quad (8)$$

$$TiO_2(e^-) + H_2O_2 \rightarrow TiO_2 + HO^- + HO^\bullet \quad (9)$$

3.2. Photocatalytic process induced by O_3 and O_3/H_2O_2

One solution for improving the performance of the photocatalytic process could be the use of oxidative agents (H_2O_2 and O_3). In the line with this and in order to evaluate the synergistic effects of O_3 and H_2O_2 with the photocalalytic process, the photocatalytic ozonation ($O_3/UV/TiO_2$) and photocatalytic perozonation ($O_3/H_2O_2/UV/TiO_2$) with a dose of 10 mM of H_2O_2 and COD concentration of 350 mg/l were also examined for treating the TCW. The COD removal efficiencies were achieved 41.1 and 49.7%, respectively for the $O_3/UV/TiO_2$ and $O_3/H_2O_2/UV/TiO_2$ processes after 240 min (Fig. 13). The BOD_5/COD ratio was also determined for the processes and obtained 0.3 and 0.4, respectively for $O_3/UV/TiO_2$ and $O_3/H_2O_2/UV/TiO_2$ processes. Similar findings related to the process ability in terms of COD conversion to BOD were reported in the literature [15,33–35]. The experiment was repeated four times and no considerable change in the results was obtained.

3.3. Photocatalytic process with regular sequence regeneration

Less effect of reaction time on the response was convinced by poisoning of the catalyst surface. Therefore, in order to prove the claim, the photocatalytic reaction was repeated with regular sequence regeneration using aeration and ozonation every 30-min period. This experiment was carried out using a raw sample of TCW with COD content of 350 mg/l and initial pH of 3. Fig. 14 compares the performance of the photocatalytic process with regular sequence regeneration by aeration and ozonation. As it can be seen in figure, the COD removal efficiencies were obtained 49 and 41%, respectively for the catalyst regenerated by sequence ozonation and aeration. As a result, the procedure could improve the process performance by about 11% increase in the COD removal efficiency. The BOD_5/COD ratio was also determined to be 0.7 and 0.4 with regular sequence regeneration with ozonation and aeration, respectively. The result was confirmed by the literatures [18].

4. Conclusion

An immobilized nanoTiO_2 PCR was successfully developed for the treatment of TCW as the novelty of the present research. This research work showed that COD mineralization and COD to BOD conversion for the TCW could be well achieved in this study. The photocatalytic process (PCR) was found time independent due to the catalyst poisoning. Combination of O_3 and O_3/H_2O_2 processes with photocatalytic process showed to be a good method to reactivate the photocatalyst. The photocatalytic process induced by O_3 and O_3/H_2O_2 showed the COD removal efficiencies of 41.1 and 49.7% after 240 min, respectively. Sequence regeneration using ozonation for de-poisoning could also improve the process performance by about 11% increase in the COD removal efficiency. The BOD_5/COD ratio was also improved to values of 0.4 and 0.7 with sequence regeneration by aeration and ozonation, respectively. It is concluded that the combination of the various AOPs with photocatalytic process (i.e. O_3 + PCR, O_3/H_2O_2 + PCR) can be an appropriate pre-treatment method prior to a biological treatment process. However, it is suggested that other possible solutions such as (O_3/H_2O_2 + PCR) system intermittently regenerated by O_3 or O_3/H_2O_2, ultrasound/O_3/H_2O_2, etc. to be examined.

Acknowledgments

The authors would like to acknowledge Kermanshah Department of Environment for providing analytical equipment to measure quality parameters. The authors would also like to acknowledge the cooperation of Mr S. Ghanbari for his fantastic and unique job in the fabrication of the immobilized photocatalytic reactor setup. Special thanks also go to Mr Kaboudi for his assistance in GC-MS analysis.

References

[1] H. Shi, Industrial wastewater—Types, amounts and effects, in: Point Sources of Pollution: Local Effects and its Control, in: Q. Yiay (Ed.), Encyclopedia of Life Support Systems, vol. 1, EOLSS, Stanford, CA, 2003, 442 p.

[2] W.D. Di Marzio, M. Sáenz, J. Alberdi, M. Tortorelli, G. Silvana, Risk assessment of domestic and industrial effluents unloaded into a freshwater environment, Ecotoxicol. Environ. Saf. 61 (2005) 380–391.

[3] M.S. Lucas, J.A. Peres, G. Li Puma, Treatment of winery wastewater by ozone-based advanced oxidation processes (O_3, O_3/UV and $O_3/UV/H_2O_2$) in a pilot-scale bubble column reactor and process economics, Sep. Purif. Technol. 72 (2010) 235–241.

[4] B. Kasprzyk-Hordern, M. Ziolek, J. Nawrocki, Catalytic ozonation and methods of enhancing molecular ozone reactions in water treatment, Appl. Catal., B 46 (2003) 639–669.

[5] A. Naldoni, A. Schiboula, C.L. Bianchi, D.H. Bremner, Mineralisation of surfactants using ultrasound and the advanced fenton process, Water Air Soil Pollut. 215 (2011) 487–495.

[6] A.K. Gupta, A. Pal, C. Sahoo, Photocatalytic degradation of a mixture of Crystal Violet (Basic Violet 3) and Methyl Red dye in aqueous suspensions using Ag^+ doped TiO^2, Dyes Pigm. 69 (2006) 224–232.

[7] N. Kannan, M. Meenakshisundaram, Adsorption of congo red on various activated carbons, a comparative study, Water Air Soil Pollut. 138 (2002) 289–305.

[8] P. Cooper, Removing colour from dyehouse waste waters—A critical review of technology available, J. Soc. Dyers Colour. 109 (1993) 97–100.

[9] Y.M. Slokar, A. Majcen Le Marechal, Methods of decoloration of textile wastewaters, Dyes Pigm. 37 (1998) 335–356.

[10] T. Robinson, G. McMullan, R. Marchant, P. Nigam, Remediation of dyes in textile effluent: A critical review on current treatment technologies with a proposed alternative, Bioresour. Technol. 77 (2001) 247–255.

[11] M. Birnie, S. Riffat, M. Gillott, Photocatalytic reactors: Design for effective air purification, Int. J. Low Carbon Technol. 1(1) (2006) 47–58.

[12] P.A. Pekakis, N.P. Xekoukoulotakis, D. Mantzavinos, Treatment of textile dyehouse wastewater by TiO_2 photocatalysis, Water Res. 40 (2006) 1276–1286.

[13] B. Nowack, T.D. Bucheli, Occurrence, behavior and effects of nanoparticles in the environment, Environ. Pollut. 150 (2007) 5–22.

[14] K. Naeem, O. Feng, Parameters effect on heterogeneous photocatalysed degradation of phenol in aqueous dispersion of TiO_2, J. Environ. Sci. 21 (2009) 527–533.

[15] R.J. Tayade, T.S. Natarajan, H.C. Bajaj, Photocatalytic degradation of methylene blue dye using ultraviolet light emitting diodes, Ind. Eng. Chem. Res. 48 (2009) 10262–10267.

[16] K.E. Sousy, A. Hussen, Kh. Hartani, Elimination of organic pollutants using supported catalysts with hydrogen peroxide, Jordan J. Chem. 2 (2007) 97–103.

[17] V. Keller, P. Bernhardt, F. Garin, Photocatalytic oxidation of butyl acetate in vapor phase on TiO_2, Pt/TiO_2 and WO_3/TiO_2 catalysts, J. Catal. 215 (2003) 129–138.

[18] S.J. Yoa, Y.S. Cho, J.H. Kim, Photocatalytic degradation of toluene with ozone addition, Korean J. Chem. Eng. 22 (2005) 364–369.

[19] H. Yaghoubi, N. Taghavinia, E.K. Alamdari, A.A. Volinsky, Nanomechanical properties of TiO_2 granular thin films, ACS Appl. Mater. Interfaces 2 (2010) 2629–2636.

[20] H. Yaghoubi, N. Taghavinia, E.K. Alamdari, Self cleaning TiO_2 coating on polycarbonate: Surface treatment, photocatalytic and nanomechanical properties, Surf. Coat. Technol. 204 (2010) 1562–1568.

[21] American Public Health Association (APHA), Standard Methods for the Examination of Water and Wastewater, twentieth ed., American Water Works Association (AWWA), Washington, DC, 1999.

[22] D. Nyangiro, New application of ozone in the treatment of chemical pulps, PhD thesis, EFPG/INPG, France, 2003.

[23] R.O. Kuehl, Design of Experiments: Statistical Principles of Research Design and Analysis, second ed., Duxbury Press, Pacific Grove, CA, 2000, pp. 2–225.

[24] A.I. Khuri, J.A. Cornell, Response Surfaces: Design and Analyses, second ed., Marcel Dekker, New York, NY, 1996.

[25] J.Ch. Sin, S.M. Lam, A.R. Mohamed, Optimizing photocatalytic degradation of phenol by TiO_2/GAC using response surface methodology, Korean J. Chem. Eng. 28 (2011) 84–92.

[26] M.A. Rauf, M.A. Meetani, S. Hisaindee, An overview on the photocatalytic degradation of azo dyes in the presence of TiO_2 doped with selective transition metals, Desalination 276 (2011) 13–27.

[27] U.I. Gaya, A.H. Abdullah, Heterogeneous photocatalytic degradation of organic contaminants over titanium dioxide: A review of fundamentals, progress and problems, J. Photochem. Photobiol., C 9 (2008) 1–12.

[28] A. Piscopo, D. Robert, J.V. Weber, Influence of pH and chloride anion on the photocatalytic degradation of organic compounds, Appl. Catal., B 35 (2001) 117–124.

[29] H. Zhu, R. Jiang, Y. Fu, Y. Guan, J. Yao, L. Xiao, G. Zeng, Effective photocatalytic decolorization of methyl orange utilizing TiO_2/ZnO/chitosan nanocomposite films under simulated solar irradiation, Desalination 286 (2012) 41–48.

[30] J.M. Poyatos, M.M. Muñio, M.C. Almecija, J.C. Torres, E. Hontoria, F. Osorio, Advanced oxidation processes for wastewater treatment: State of the art, Water Air Soil Pollut. 205 (2010) 187–204.

[31] A. Safarzadeh-Amiri, O_3/H_2O_2 treatment of methyl-tert-butyl ether (MTBE) in contaminated waters, Water Res. 35 (2001) 3706–3714.

[32] E.S. Elmolla, M. Chaudhuri, Photocatalytic degradation of amoxicillin, ampicillin and cloxacillin antibiotics in aqueous solution using UV/TiO_2 and $UV/H_2O_2/TiO_2$ photocatalysis, Desalination 252 (2010) 46–52.

[33] F.J. Beltrán, A. Aguinaco, J.F. García-Araya, A. Oropesa, Ozone and photocatalytic processes to remove the antibiotic sulfamethoxazole from water, Water Res. 42 (2008) 3799–3808.

[34] M. Muruganandham, M. Swaminathan, TiO_2–UV photocatalytic oxidation of Reactive Yellow 14: Effect of operational parameters, J. Hazard. Mater. 135 (2006) 78–86.

[35] Q. Hong, S. De-zhi, CH. Guo-qing, Formaldehyde degradation by $UV/TiO_2/O_3$ process using continuous flow mode, J. Environ. Sci. 19 (2007) 1136–1140.